Analyst

Accepted Manuscript

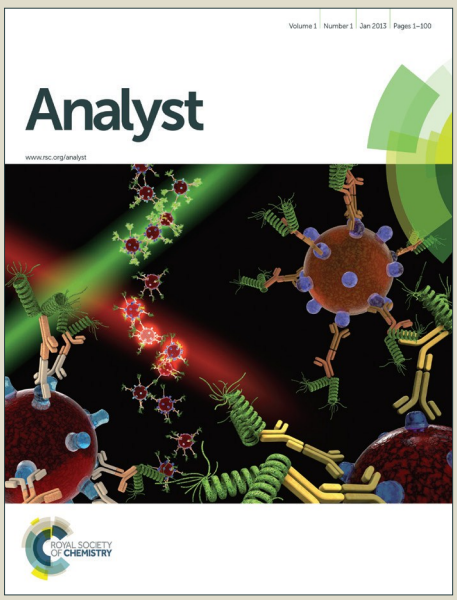

ROYAL SOCIETY OF CHEMISTRY

www.rsc.org/analyst

Journal Name

ARTICLE

Sensitive electrochemical detection of nitric oxide based on AuPt and reduced graphene oxide nanocomposites

Received 00th January 20xx,
Accepted 00th January 20xx

DOI: 10.1039/x0xx00000x

www.rsc.org/

Zhonggang Liu,[a] Heidi Forsyth,[b] Neelam Khaper[b] and Aicheng Chen*[,a]

Since nitric oxide (NO) plays a critical role in many biological processes, its precise detection is essential toward an understanding of its specific functions. Here we report on a facile and environmentally compatible strategy for the construction of an electrochemical sensor based on reduced graphene oxide (rGO) and AuPt bimetallic nanoparticles. The prepared nanocomposites were further employed for the electroanalysis of NO using differential pulse voltammetry (DPV) and amperometric methods. The dependence of AuPt molar ratios on the electrochemical performance was investigated. Through the combination of the advantages of the high conductivity from rGO and highly electrocatalytic activity from AuPt bimetallic nanoparticles, the AuPt-rGO based NO sensor exhibited a high sensitivity of 7.35 μA μM^{-1} and a low detection limit of 2.88 nM. Additionally, negligible interference from common ions or organic molecules was observed, and the AuPt-rGO modified electrode demonstrated excellent stability. Moreover, this optimized electrochemical sensor was practicable for efficiently monitoring the NO released from rat cardiac cells, which were stimulated by L-arginine (L-arg), showing that stressed cells generated over 10 times more NO than normal cells. The novel sensor developed in this study may have significant medical diagnostic applications for the prevention and monitoring of disease.

Introduction

Nitric oxide (NO), which has been found to be released by various cells in mammalian systems, plays an important role in many biological processes, such as vasodilation, blood pressure, neurotransmission, immune response, and as a cytostatic agent.[1,2] The accurate measurement of NO is of benefit to understand its essential function in such physiological processes as neurotransmission, platelet aggregation, macrophage function, and vasodilation.[3,4] Owing to its importance and relevance in biological processes, there has been increasing interest in the research and development of efficient analytical techniques for the sensitive measurement of NO.

To date, various analytical methods have been explored for the determination of NO, including chemiluminescence,[5,6] fluorescent probe.[7,8] electrospray ionization mass spectrometry (ESI-MS),[9] X-ray photoelectron spectroscopy, gas sensor,[10] and reverse-phase high performance liquid chromatography.[11] However, these approaches are time-consuming and costly, requiring complicated sample preparation and expensive instrumentation. Alternatively, the development of electrochemical sensors has gained great attention due to its merits in terms of high sensitivity, easy-use, and low cost, which have been employed in a wide range of fields, especially in clinical or biomedicine.[12-17]

Cho et al. fabricated PAH-AuNP/PAA-AuNP multilayers with cationic poly(allylamine hydrochloride) (PAH) and anionic poly(acrylic acid) (PAA), where the porous structure exhibited high electrochemical activity toward NO.[18] Yang et al. focused on the basic redox heme protein, cytochrome c (Cyt c), which was immobilized onto sodium dodecyl sulfate (SDS), L-cysteine. The assembled biosensors displayed high electrocatalytic activity for NO.[19,20] Other electrochemical sensors integrating porphyrin or phthalocyanine with Cu(II),[21] Ni(II),[22] Fe(II),[23] or Pt(II),[24] enzymes (catalase, superoxide dismutase, etc.),[25] carbon based nanocomposites,[26-28] and polymer membranes[29] for the detection of NO have been explored as well. It is worthy to mention that although satisfying results might be obtained for the analysis of NO, these electrochemical sensors necessitated complex fabrication procedures, or expensive and fragile enzymes, leading to limited applications. Thus, it is still a great challenge and of importance to explore the novel and simple techniques for the fabrication of efficient electrochemical sensors.

In the present work, we report on a facile strategy for the fabrication of electrochemical sensors with AuPt-rGO nanocomposites, where the nanocomposites were directly deposited onto a glassy carbon electrode (GCE) surface. Herein rGO was prepared via the electrochemical reduction of

[a] Department of Chemistry, Lakehead University, 955 Oliver Road, Thunder Bay, Ontario P7B 5E1, Canada. E-mail: aicheng.chen@lakeheadu.ca (A. Chen).Tel.:+1 807 3438318; Fax: +1 807 3467775.
[b] Northern Ontario School of Medicine, Lakehead University, 955 Oliver Road, Thunder Bay, Ontario, P7B 5E1, Canada.

†Electronic Supplementary Information (ESI) available: SEM images of Au-rGO and Pt-rGO (Fig. S1); characterization of bare GCE and modified electrodes in 0.1 M H_2SO_4 solution (Fig. S2); DPV and amperometric responses of bare GCE and modified electrodes toward NO (Figs. S3 and S4); real sample tests (Fig. S5); a comparison of electrochemical performance of the different modified electrodes towards NO (Table S1). See DOI: 10.1039/x0xx00000x

graphene oxide, which not only improves electron transfer, but also offers a favorable substrate for dispersion and stabilization of various metal nanoparticles.[30-32] Bimetallic AuPt nanoparticles were in particular focus due to their capacity for improved catalytic properties, relative to their constituent metals.[33-36] The effect of the composition of the AuPt nanoparticles on the catalytic oxidation of NO was investigated; and the optimized AuPt-rGO nanocomposites showed remarkable sensitivity, selectivity and stability for the electrochemical sensing of nitric oxide. The developed AuPt-rGO nanocomposite sensor was further employed for the amperometric detection of NO released from normal and stressed rat cardiac cells.article.

Experimental

Chemical reagents

All chemicals were of analytical grade and used as received without any further purification. L-arginine (L-arg), L-cysteine, ascorbic acid, uric acid, NaH_2PO_4, Na_2HPO_4, graphene oxide (GO), and gold(III) chloride trihydrate were purchased from Sigma-Aldrich. Phosphate buffer saline (PBS) solutions (0.1 M) were prepared by using 0.1 M NaH_2PO_4, Na_2HPO_4, and 0.1 M NaCl. All water was obtained from a NANO pure® Diamond™ UV ultrapure water purification system (18 MΩ cm).

Preparation of NO samples

The saturated NO in a PBS solution was prepared as previously reported.[37] In brief, a 0.1 M PBS solution was purged with high-purity argon gas for 30 min to remove oxygen, after which the solution was bubbled with pure NO gas for 30 min to prepare a NO saturated solution. The concentration of saturated NO solution at room temperature was reported to be 1.8 mM. All NO standard solutions were prepared daily by the appropriate dilution of the stock solution.

Fabrication of the AuPt-rGO modified electrodes

Prior to modification, a bare glassy carbon electrode (GCE, 3 mm in diameter) was polished with 0.3 µm, 0.05 µm alumina power slurries to a mirror-shiny surface and then sonicated with HNO_3 solution (v:v 1:1), absolute ethanol and deionized water, respectively.[38] In the present work, a facile two-step electrochemical process was employed to prepare an AuPt-rGO modified GCE (Scheme 1). Firstly, a 5 µL suspension of GO (0.3 mg mL^{-1}) was cast on a GCE and allowed to air dry. Subsequently, the cast GO was electrochemically reduced to a rGO film via cyclic voltammetry scanning for 20 cycles in a 0.1 M PBS solution, which was carried out in the potential range between 0.0 and -1.5 V vs Ag/AgCl at a scan rate of 50 mV s^{-1}.[39] Secondly, the AuPt nanoparticles were in situ electro-synthesized on the rGO/GCE by applying -250 mV for 500 s in an aqueous solution of 0.1 M H_2SO_4 that contained different Au/Pt molar ratios (the total concentration of $AuCl_3$ and H_2PtCl_6 was maintained at 4 mM). The resulting electrode (denoted as AuPt-rGO/GCE) was subsequently rinsed with water and used for further measurements.

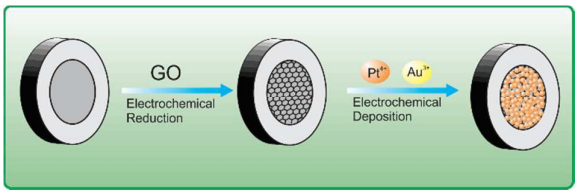

Scheme 1. An illustration for the fabrication of the AuPt-rGO nanocomposite modified glassy carbon electrode.

Instrumentation

Electrochemical experiments were recorded using a CHI 660B computer-controlled potentiostat (CH Instrument Inc., USA) with a standard three electrode system. A bare GCE or modified GCE served as a working electrode; an Ag/AgCl (3 M KCl) electrode as the reference electrode, and a platinum coil as the counter electrode. Scanning electron microscopic images were obtained through the use of field emission scanning electron microscopy (FE-SEM, Hitachi SU-70), equipped with energy dispersive X-ray spectrometry (EDS), which was employed to determine the composition of AuPt nanoparticles deposited on the rGO thin film. X-ray diffraction (XRD) patterns were recorded via a PhilipsX'Pert Pro X-ray diffractometer with Cu Kα radiation (1.5418 Å).

Electrochemical experiments

Differential pulse voltammetry (DPV) was used for the detection of NO in a 0.1 M PBS solution (pH 7.2). The DPV responses were recorded between 0.2 and 1.0 V with increased E of 0.004 V, amplitude of 0.05 V, pulse width of 0.2 s, sampling width of 0.0167 s, and pulse period of 0.5 s. All solutions were deaerated with high-purity argon for 20 min prio to the recording of the voltammograms. All experiments were conducted at room temperature (20 ± 2^{o}C).

Preparation and detection of rat cardiac cells

Rat cardiac cells (H9C2 cells; ATCC) were cultured in Dulbecco's Modified Eagle's Medium (DMEM, Sigma Aldrich, St. Louis, MO, USA) supplemented with 10% fetal bovine serum (FBS) and an antibiotic/antimycotic (100 units mL^{-1} penicillin G sodium, 100 µg mL^{-1} streptomycin sulfate, 0.25 µg mL^{-1} amphotericin B). The cells were grown in two T-150 flasks in a humidified atmosphere (37°C and 5% CO_2), and harvested when they reached 80-85% confluency. One flask was treated with 5 mM H_2O_2 for 1 h prior to being harvested while the other was left untreated (control, used as normal cells). The cells were counted using a hemocytometer prior to exposure to the probe, where the concentration of cells was 1,656,000 cells/mL in the control flask and 71,700 cells/mL in the treated flask. For amperometric measurement, 10 mM L-arg was added to 10 mL PBS solution. The applied potential of 0.84 V was used in the amperometric measurements under a stirred condition. During the experiment, rat cardiac cell smaples was successively added into the solution and the amperometric curve was recorded.Results and discussion.

Results and discussion

Surface characterization of the AuPt-rGO nanocomposites

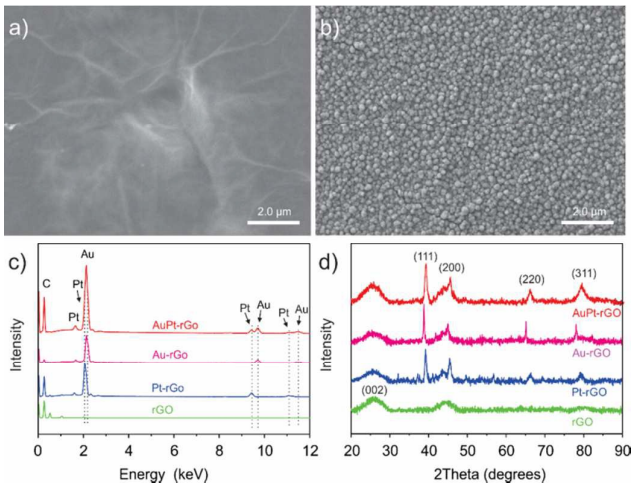

Fig. 1 SEM images of (a) rGO and (b) AuPt-rGO nanocomposites (with the Au:Pt ratio of 64:36). (c, d) EDS spectra and XRD patterns of rGO, Pt-rGO, Au-rGO, and AuPt-rGO.

The AuPt nanoparticles electrodeposited on rGO were initially characterized by SEM. As shown in Fig. 1a, the GCE surface was uniformly covered by the electrochemically reduced rGO sheets. Following the electrodeposition, dense AuPt nanoparticles were homogeneously formed on the rGO sheets as seen in Fig. 1b. An obvious morphological change may be observed for the bimetallic AuPt nanoparticles in contrast to mono Au nanoparticles (Fig. S1a and b) and Pt nanostructure (Fig. S1c and d). Fig. 1c displays the EDS spectra of the formed rGO, Pt-rGO, Au-rGO and AuPt-rGO nanocomposites. Strong Au and Pt peaks at ~2.10 keV as well as weak peaks at ca. 9.55 and 11.3 keV appeared in the EDS spectrum of the AuPt-rGO nanocomposite, Further qualitative analysis of the EDS spectrum revealed that the ratio of Au:Pt of the formed nanocomposite was 64:36, which was close to the Au/Pt molar ratio 60:40 in the electrolyte used for the electrodeposition.

Fig. 1d compares XRD patterns of the as-prepared rGO, Pt-rGO, Au-rGO and AuPt-rGO samples. For rGO, the peak at 25.8 reflects the carbon (002) due to the formation of rGO on the electrode substrate via an electrochemical reduction method.[40,41] The XRD patterns of Au and Pt nanoparticles may be indexed to face centered-cubic (fcc) Au(JCPDS 04-0784) and Pt(JCPDS 04-0802).[42] The peaks at ca. 38.5, 44.8, 65.1, and 78.0 may be indexed to Au (111), (200), (220), and (311) diffraction peaks, respectively, while the peaks at ca. 39.3, 45.7, 66.9, and 79.2 to Pt (111), (200), (220), and (311) peaks, respectively, confirming that the as-prepared Pt and Au nanoparticles had a highly crystalline phase. In comparison with the XRD patterns of Au and Pt nanomaterials electrochemically deposited on the rGO sheets, the highly crystalline of the formed AuPt nanoparticles was also witnessed. The absence of the separated Au and Pt peaks and the condensation of Pt and Au crystalline revealed that the AuPt alloy nanoparticles were produced via such a facial electrodeposition method. The well-resolved peaks may be assigned to (111), (200), (220), and (311), respectively, for the alloy AuPt nanoparticles.

Electrochemical study of the AuPt-rGO nanocomposites

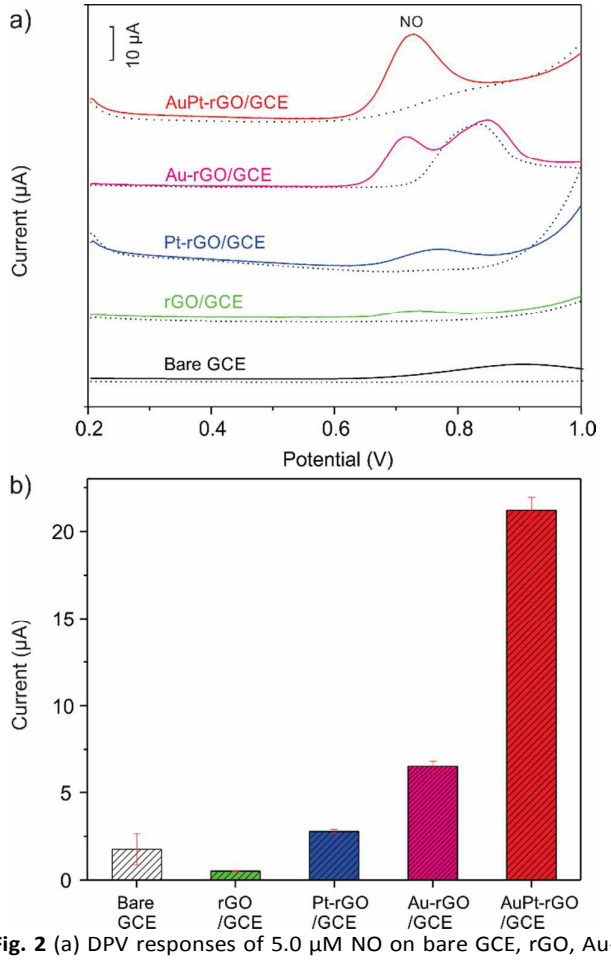

Fig. 2 (a) DPV responses of 5.0 μM NO on bare GCE, rGO, Au-rGO, Pt-rGO, and AuPt-rGO modified GCE in 0.1 M PBS (pH 7.2). (b) The corresponding responses of the different modified electrodes.

Fig. S2 presents the cyclic voltammograms (CVs) of the bare GCE and the GCE modified with the rGO, Pt-rGO, Au-rGO and AuPt-rGO nanomaterials recorded in a 0.1 M H_2SO_4 solution at a scan rate of 50 mV s^{-1}. As expected, featureless CV was obtained for the bare GCE. After the modification with rGO, the capacitance of the electrode was increased. Strong hydrogen adsorption and desorption as well as Pt oxide formation and reduction peaks were observed for the Pt-rGO/GCE, while strong Au oxide formation and reduction peaks appeared in the CV of the Au-rGO/GCE. In comparison to the Au-rGO and Pt-rGO modified GC electrodes, the obvious electrochemical reduction peaks at +0.40 V and +0.82 V, corresponding to the reduction of the Pt and Au oxides, respectively,[37,40] further confirmed that the AuPt nanoparticles had been electrodeposited onto the GCE surface. The electrochemically active surface area (ESCA) of the Pt-rGO, Au-

rGO and AuPt-rGO modified electrodes was estimated, based on the hydrogen adsorption/desorption on Pt and oxide formation/reduction on Au,[43,44] to be 1.17, 0.97 and 1.29 cm^2, respectively, which were 16.6, 13.7 and 18.3 times higher than the geometric surface area of the GCE substrate (0.0706 cm^2). These results indicated that the GCE surface was well covered with the Pt-rGO, Au-rGO and AuPt-rGO nanocomposites, which was consistent with the SEM images (Fig. 1b and Fig. S1).

The electrocatalytic activity of the AuPt-rGO nanocomposites toward NO oxidation was investigated using DPV technique. Fig. 2a displays the DPV responses of a bare GCE and the GCEs modified with the rGO, Au-rGO, Pt-rGO, and AuPt-rGO nanomaterials to 5.0 μM NO (Solid lines). For comparison, their DPVs recorded in 0.1 M PBS (pH 7.2) in the absence of NO were also included in Fig. 2a (dotted lines). Although the responses of the GCE and rGO/GCE were small, the peak potential for NO oxidation was negatively shifted from 0.908 to 0.744 V after being modified with the rGO. The current response was improved with the Pt-rGO and Au-rGO nanocomposites. Interestingly, with the AuPt-rGO nanocomposite, a well-defined peak for NO oxidation appeared at +0.724 V with a much higher peak current, which was nearly seven-fold and three-fold higher than that of the GCEs modified with Pt-rGO, and Au-rGO, respectively (Fig. 2b).

Subsequently, the effects of the different Au/Pt molar ratios in the AuPt-rGO nanocomposites were further investigated. The morphology of the synthesized AuPt-rGO nanocomposites with different Au/Pt molar ratios was similar as seen in Fig. 1b. Their DPV curves (except the Au/Pt ratios of 0:100 and 100:0) recorded in a 0.1 M PBS in the absence (dotted line) and in the presence of 5.0 μM NO are displayed in Fig. 3a, and their corresponding peak current and potential by varying the Au/Pt molar ratios are presented in Fig. 3b. No obvious change in the voltammetric shape was observed through the change of the Au/Pt molar ratios. The current response was increased with the increase of the Au/Pt molar ratio from 0.0:100 to 64:36; but it was decreased with the further increase of the percent of Au, revealing that the highest current response was attained with the Au/Pt ratio of 64:36. It is worthy to note that the peak potential for the NO oxidation on the AuPt-rGO nanocomposites was slightly decreased from +0.756 to +0.712 V with the increase of the Au:Pt ratio from 0.0% to 100%. It is well-known that, in voltammetric experiments, the electrode potential provides thermodynamic information on electrochemical reactions, whereas the current represents the reaction rate.[45] The aforementioned results suggest that the electrochemical oxidation of NO at the Au-rGO/GCE is subject to the kinetic limitation, and that the formation of AuPt bimetallic AuPt-rGO nanocomposites significantly increased the current response, leading to an efficient synergy effect due to the modification of the surface electronic structure.[46]

DPV detection of NO

Differential pulse voltammetry, which can suppress the noise to improve the signal-to-noise ratio (S/N), was applied to investigate the electrochemical performance of the GCE

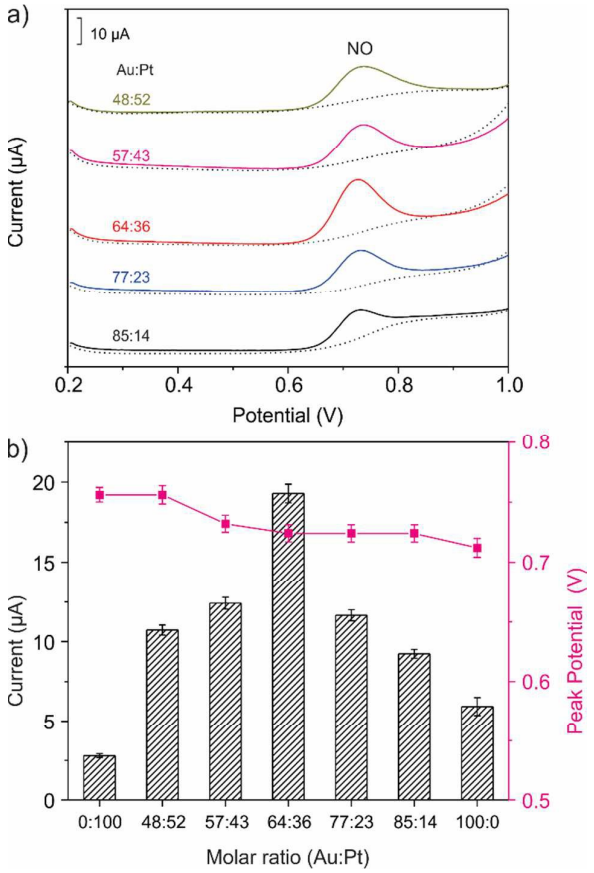

Fig. 3 (a) DPV responses of AuPt-rGO/GCE with different Au/Pt molar ratios toward 5.0 μM NO in a 0.1 M PBS solution (pH 7.2). (b) Dependence of peak current and corresponding peak potential of 5.0 μM NO on the different Au/Pt molar ratios of the AuPt-rGO modified electrode. Error bars represent the standard deviation over three consecutive measurements.

modified with the optimized AuPt-rGO nanocomposites toward the detection of NO. Fig. 4a displays a series of the DPV curves recorded in a 0.1 M PBS solution (pH 7.2), where the NO concentration was varied from 0.0 to 10 μM. A well-defined oxidation peak at +0.724 V was observed, which is obviously lower than that reported in the literature,[37,47] suggesting that the AuPt-rGO modified electrode exhibited a far improved electrocatalytic oxidation activity toward NO. The peak currents increased in a linear manner against NO concentrations, which was ascribed to the oxidation of NO to HNO_2.[48] There were two segments in the relevant linear range for the detection of NO, which were 0.02 – 1.8 μM, and 2.0 – 10 μM as shown in Fig. 4b. The obtained sensitivities were 6.73 μA $μM^{-1}$ and 2.67 μA $μM^{-1}$ with the coefficient factors (R^2) of 0.992 and 0.988, respectively. The limit of detection (LOD) was calculated to be 3.69 nM (S/N of 3). For comparison, the electrochemical performance of the bare GCE and the GCE modified with the rGO, Pt-rGO, and Au-rGO nanomaterials was also evaluated with DPV under the identical conditions, as shown in Fig. S3. The corresponding sensitivities were determined to be 0.351, 0.122, 0.494, and 1.39 μA $μM^{-1}$, respectively.

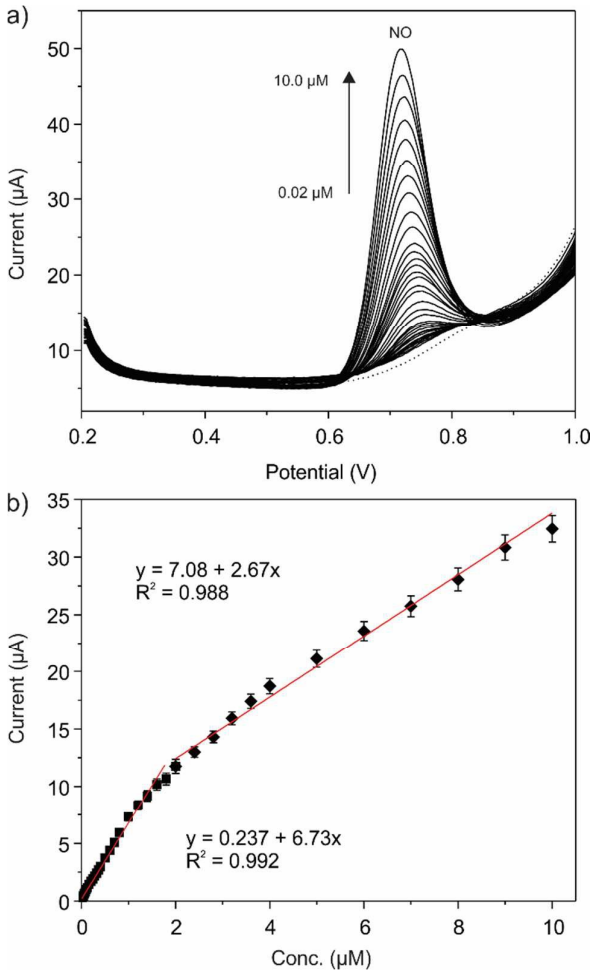

Fig. 4 (a) DPV responses of an AuPt-rGO modified electrode toward NO with different concentrations in a 0.1 M PBS solution (pH 7.2), where the dotted line refers to the baseline. Increased E of 0.004 V, amplitude of 0.05 V, pulse width of 0.2 s, sampling width of 0.0167 and pulse period of 0.5 s. (b) The corresponding calibration plots between the DPV response and NO concentration (n = 3).

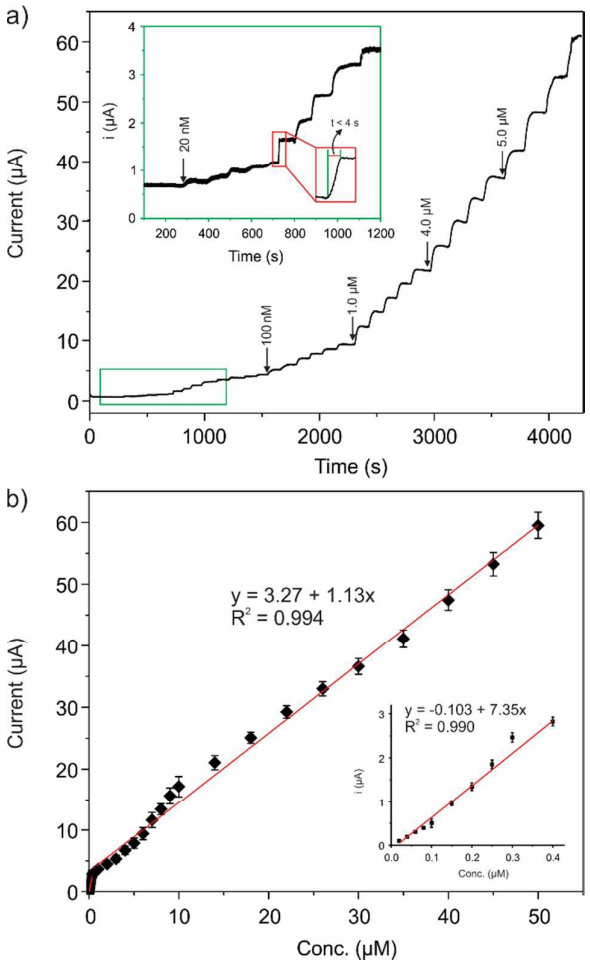

Fig. 5. (a) Amperometric responses of the AuPt-rGO modified electrode with the successive addition of NO, from 0.02 μM to 50 μM, in a 0.1 M PBS solution (pH 7.2) at an applied potential of +0.84 V. The inset is the enlarged amperometric responses of NO under a low concentration. (b) The calibration plot of the response current as a function of the concentrations of NO (n = 3).

Amperometric Detection of NO

Fig. 5 presents a typical hydrodynamic amperometric NO response of the GCE modified with the optimized AuPt-rGO nanocomposite, which was carried out based on the successive addition of NO with different concentrations in a well-stirred solution of 0.1 M PBS (pH 7.2), whereas the inset is the magnified amperometric response curve at the low NO concentration range. Clearly, the AuPt-rGO modified electrode exhibited a rapid and sensitive response to changes in NO concentrations, and the response time determined from the inset of Fig. 5a was less than 4 s, to achieve 95% of steady-state current. An obvious increase in the oxidation current was observed with the successive addition of NO. Fig. 5b presents the calibration curve in the linear response over the concentration range from 20 nM to 400 nM, and from 400 nM to 50 μM, with corresponding sensitivities of 7.35 μA μM^{-1} and 1.13 μA μM^{-1}. The two calibration plots with higher sensitivity in the low concentration range and lower sensitivity in the high concentration range might be ascribed to the increase of the adsorption of the oxidized species at the electrode surface when the concentration of NO was high, thus decreasing the rate of the electrochemical oxidation of NO. The calculated LOD was 2.88 nM (S/N = 3). Under the same conditions, the electrochemical performance of the bare GCE and the GCEs modified with rGO, Pt-rGO, and Au-rGO nanomaterials was also examined with amperometric method as shown in Fig. S4. An overall comparison of the electrochemical performance of the bare GCE and the GCE modified with the rGO, Au-rGO, Pt-rGO, and AuPt-rGO nanomaterials toward the detection of NO is presented in Table S1. Obviously, the AuPt-rGO nanocomposites exhibited a wider linear range, higher sensitivities and lower LOD toward the electrochemical detection of NO. The electrochemical performance was significantly improved over the other modified electrodes.

A further comparison of the electrochemical performance of the optimized AuPt-rGO nanocomposites developed in the present study with the electrochemical NO sensors reported in the literature is summarized in Table 1. To date, for the electrochemical sensing of NO, much work has been invested in the development of various modified electrodes, including Hb/GNPs-GR-SDS BPG, $(PAH\text{-}AuNP/PAA\text{-}AuNP)_n$ modified ITO, CAS/SOD/MP/MWCNT-PTTCA/AuNPs modified GCE.[18,25,49] However, these methods required complex fabrication procedures or expensive and fragile enzymes. Although the electrochemical detection of NO with Au@Pt core-shell nanoparticles modified graphene paper has been reported, complicated synthetic and assembly procedures were applied for the Au@Pt nanoparticles and the modified electrode.[50] In contrast to previous literature as relates to the electrochemical sensing of NO, it was demonstrated that the novel AuPt-rGO nanocomposite, fabricated in a simple way, exhibited high sensitivity and low LOD for the effective detection of NO.

Table 1 Comparison of the Modified Electrodes for the Electrochemical Determination of NO

Electrode (dimension)	Method	Electrolyte (pH)	Linearity range (μM)	Sensitivity ($\mu A\ \mu M^{-1}$)	LOD (nM)	Ref.
(PAH-AuNP/PAA-AuNP)$_n$/ITO (--)	CV	PBS (3.0)	1000 – 20000			18
CAS/SOD/MP/MWCNT-PTTCA/AuNPs/GCE (3 mm dia.)	CV, Amperometry	0.1 M PBS (4.0)	1– 40	1.1 ± 0.01	4.3±0.2	25
Nafion-Au film/GCE (3 mm dia.)	CV, LSV, Amperometry	0.1 M PBS (2.5)		~ 0.313	1.0	29
RGO-Au nanorod in silicate sol–gel matrix (3 mm dia.)	CV, LSV,Amperometry	0.1 M PBS (7.2)	0.01 – 0.14	0.598	6.5	37
AuNPs/ITO (0.0314 cm^2)	CV, Amperometry	Na_2HPO_4–citric acid buffer solution (2.2)	1 – 500	1.22×10^{-3}	670	47
Hb/GNPs-GR-SDS/BPG (5.2 mm dia.)	CV, Amperometry	0.1 M PBS (7.0)	0.72–7.92		12	49
Au-RGO/GCE (--)	CV, Amperometry	PBS (7.4)	25 – 200	0.921	133	51
rGO-Co_3O_4@Pt/GCE (3 mm dia.)	Amperometry	0.1 M PBS (2.5)	10 – 650	0.026 ± 0.0002	1730	52
SWCNT-RTIL/nafion Pt microelectrode (100 μm dia.)	DPV	100 mM NaCl +10 mM PBS (7.4)	0.1 – 100	0.0436	100	53
Graphene-nafion/GCE	SWV	0.1 M PBS (2.5)	50 – 450	0.062	11.61×10^3	54
3D graphene-ILs/nafion/GCE (3 mm dia.)	CV, Amperometry	0.1 M PBS (7.0)	0.8 – 16	0.795	16	55
MWCNTs-nafion/GCE (--)	CV, Amperometry	0.1 M PBS (7.0)	0.2 –150	~ 0.3	80	56
Bi-layer AuNPs/GCE (0.28 cm^2)	CV, Amperometry	PBS (1.92)	0.05 –10	~ 0.463	27	57
AuNPs-MPTS/ITO (0.24 cm^2)	CV, Amperometry	0.2 M PBS (2.0)	0.012 – 700	~ 0.25	0.31	58
EDAS(TiO_2-Au)$_{nps}$ (3 mm dia.)	SWV	0.1 M PBS (2.5)	1 – 60		1000	59
NiTMHPP/Carbon fiber (7 μm dia.)	CV, Amperometry	PBS (7.4)			2-3	60
Nano-Au colloid-Nafion film/Pt microelectrode (200 μm dia)	DPV, DPA	HBSS	0.1 – 40		50	61
AuPt-rGO/GCE (3 mm dia.)	CV, DPV, Amperometry	0.1 M PBS (7.2)	0.02 – 0.4 0.4 – 50	7.35 ± 0.26 1.13 ±0.05	2.88 ± 0.13	This work

Dia.: diameter; PAH: poly(allylamine hydrochloride); PAA: anionic poly(acrylic acid); BPG: basal plane graphite electrode; ITO: Indium tin oxide electrode; GCE: glassy carbon electrode; CAS: Catalase; SOD: superoxide dismutase; MP: microperoxidase; PTTCA: poly-5,2:5,2-terthiophene-3-carboxylic acid; SWCNT: single-walled carbon nanotube; Hb: hemoglobin; SDS: sodium dodecyl sulfate; ILs: ionic liquids; MPTS: (3-mercaptopropyl)-trimethoxysilane; NiTMHPP: nickel tetrakis(3-methoxy-4-hydroxyphenyl)porphyrin; HBSS: Hank's balanced salt solution

Interference study

Since nitrite anions (NO_2^-) typically exist at higher concentrations than that of NO in actual systems, they have close oxidation potentials; hence the possible interference

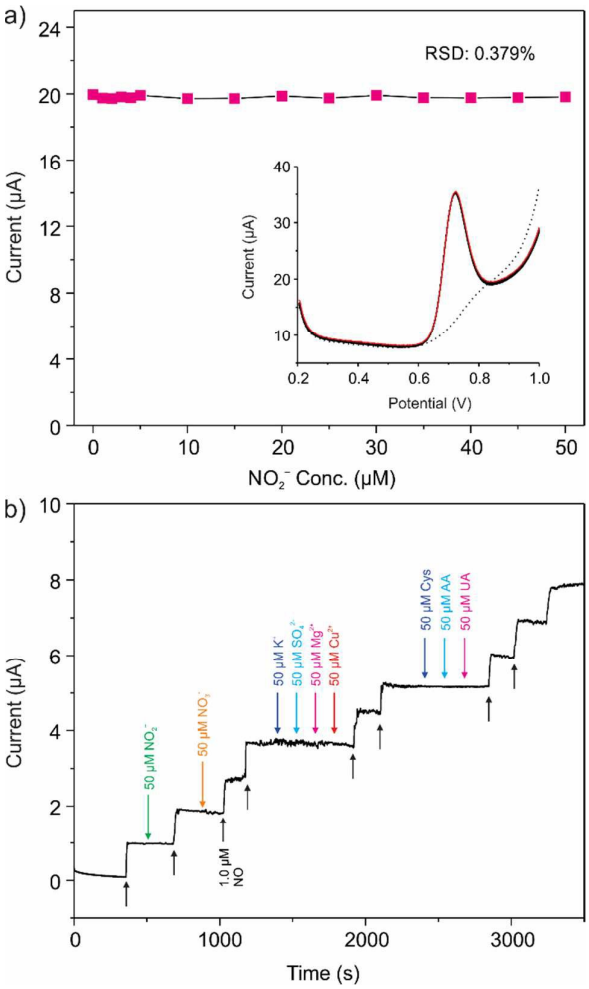

Fig. 6 (a) The influence of NO_2^- on DPV responses of 5.0 μM NO in a 0.1 M PBS (pH 7.2) solution with different concentrations of NO_2^-. Data were collected from every DPV response at +0.724 V shown in the inset. The red curve represents the voltammogram of 5.0 μM NO in the absence of NO_2^-. (b) Amperometric curve obtained on an AuPt-rGO modified electrode for the successive addition of 1.0 μM NO, and each 50 μM of NO_2^-, NO_3^-, K^+, SO_4^{2-}, Mg^{2+}, Cu^{2+}, Cys, AA, and UA in 0.1 M PBS (pH 7.2). Applied potential: +0.84 V.

from NO_2^- was emphasized and carefully tested in this study. Fig. 6a presents the DPV response of the optimized AuPt-rGO nanocomposites to 5.0 μM NO in a 0.1 M PBS (pH 7.2) solution with the increase of the concentrations of NO_2^- from 0.0 to 50 μM Interestingly, with the successive addition of various concentrations of NO_2^-, there was no apparent change in the current response, even though 10-fold more of NO_2^- than NO was introduced into the same solution, where the obtained relative standard deviation (RSD) was 0.379%. Moreover, no change on the peak potential of NO oxidation was observed (Inset in Fig. 6a). This was further confirmed by the amperometric tests, as displayed in Fig. 6b; there was no obvious current response following the addition of NO_2^- to the testing solution. The consistent response to the successive addition of 1.0 μM NO was clearly observed in the presence of

50 μM NO_2^- (Fig. 6b). Similarly, other common interfering species, such as NO_3^-, K^+, SO_4^{2-}, Mg^{2+}, Cu^{2+}, L-cysteine (Cys), ascorbic acid (AA), and uric acid (UA) were also systematically evaluated as shown in Fig. 6b. The test results demonstrated that the AuPt-rGO nanocomposites sensor developed in this study exhibited a favorable anti-interference capacity and selectivity characteristics. No obvious interference was observed from AA, Cys, UA and NO_2^-, which may be attributed to the low kinetics of the adsorption and electrochemical oxidation of these species on the AuPt-rGO modified electrode.

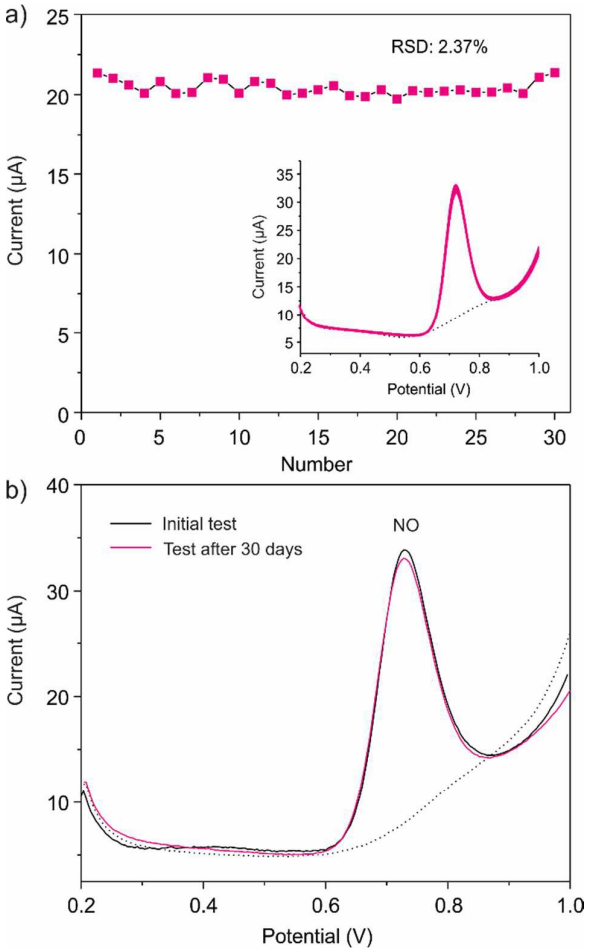

Fig. 7 Measurement stability in the presence of 5.0 μM NO in 0.1 M PBS (pH 7.2) on an AuPt-rGO modified electrode. Data were collected from every DPV response at +0.724 V shown in the inset. The dotted line refers to the baseline. (b) DPV response of 5.0 μM NO at the modified electrode measured after being stored for 30 days (red line).

Stability measurement

Repetitive measurements by DPV were carried out to characterize the stability of the AuPt-rGO modified electrode. Fig. 7 depicts the current responses to 5.0 μM NO over 30 cycles. Data were collected from every DPV response at +0.724 V (Fig. 7 inset). No apparent change in the current responses was observed, and the relative standard deviation (RSD) was 2.37%. It was also found that no shift appeared in the peak potential. The long-term stability of the AuPt-rGO modified electrode was further evaluated after storage for 30 days, where the current response was only slightly decreased (less than 3%) in comparison with the initial measurement (Fig. 7b). This revealed that the AuPt-rGO modified electrode, assembled in such simple manner, possessed robust performance under the repeated measurements without any obvious loss in response.

Amperometric sensing of NO released from normal and stressed rat cardiac cells

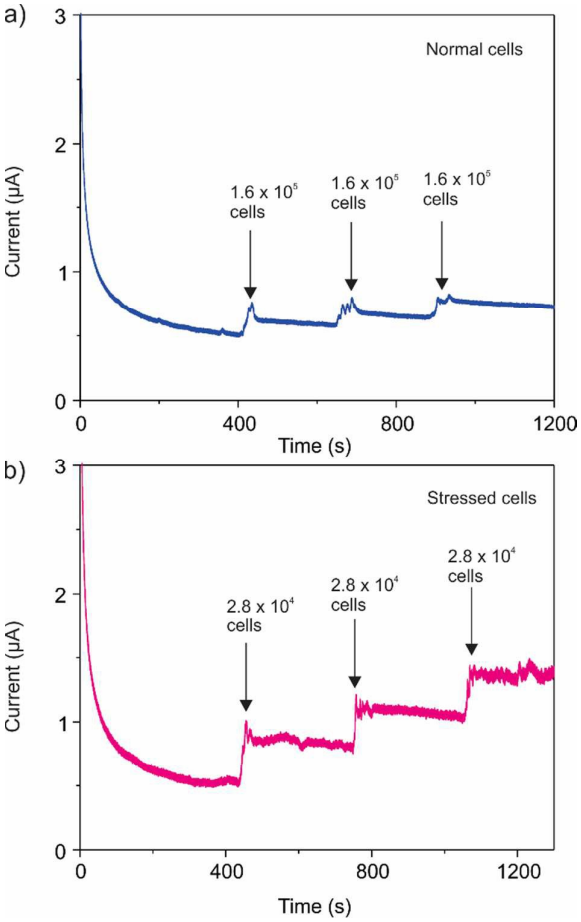

Fig. 8 Amperometric responses of NO release by the addition of different amount of (a) normal cells and (b) stressed cells in the presence of 10 mM L-Arg in a 0.1 M PBS solution (pH 7.2). Applied potential: +0.84 V.

It is recognized that NO plays a critical role in the control of many cellular and organ functions and that it can be biosynthesized from L-arg in the presence of nitric oxide synthetase (NOS). In the presence of L-arg, the NOS in rat cardiac cells may convert L-arg into L-citrulline and NO. To demonstrate a practical application, the developed sensor was utilized to monitor NO release from rat cardiac cells. As seen in Fig. S5, the developed AuPt-rGO electrode showed no response to L-arg, and negligible response to the addition of the rat cardiac cells in the absence of L-arg. Fig. 8a and b

present the amperometric responses to the addition of the normal and stressed rat cardiac cells into 0.1 M PBS solution containing 10 mM L-arg, respectively. A rapid and linear current response was observed with increasing quantities of the normal and stressed rat cardiac cells. The concentrations of NO release from the normal and stressed cells were estimated to be 33.1±1.80 nM and 57.3±2.14 nM, respectively. Interestingly, although the number of stressed cells ($2.8x10^4$) was 5.7 times lower than that of the normal cells ($1.6x10^5$), the amount of NO release from the stressed cells was over 10 times more NO than normal cells. These results indicated that this novel electrochemical sensor has strong potential for the effective detection of this significant biomarker in biological processes, which may have important implications for medical diagnostics.

Conclusions

In summary, we have successfully fabricated a new electrochemical sensor by the integration of rGO and AuPt bimetallic nanoparticles via a facile and environmentally compatible approach. The AuPt-rGO nanocomposites were optimized and investigated for the detection of NO, showing high sensitivity (7.35 μA μM^{-1}), low LOD (2.88 nM) and high stability. No obvious interference from NO_2^-, NO_3^-, cysteine, AA, UA, or other common ions was observed. In addition, this novel electrochemical sensor demonstrated the sensitive detection of the NO released from rat cardiac cells, revealing that stressed rat cardiac cells generated considerably more NO than the normal cells. Although Au and Pt are precious metals, the total amount of Au and Pt used for each sensor was very small. The sensor developed in this study may serve as an important and cost-effective tool for the study of cellular stress responses in biological processes and for medical diagnostics.

Acknowledgements

This work was supported by a Discovery grant from the Natural Sciences and Engineering Research Council of Canada (NSERC RGPIN-2015-06248). A.C. acknowledges NSERC and the Canada Foundation for Innovation (CFI) for the Canada Research Chair Award in Materials and Environmental Chemistry.

Notes and references

1 R. M. J. Palmer, D. S. Ashton and S. Moncada, *Nature*, 1988, **333**, 664-666.
2 E. Southam and J. Garthwaite, *Neuroreport*, 1991, **2**, 658-660.
3 R. F. Eich, T. S. Li, D. D. Lemon, D. H. Doherty, S. R. Curry, J. F. Aitken, A. J. Mathews, K. A. Johnson, R. D. Smith, G. N. Phillips and J. S. Olson, *Biochemistry*, 1996, **35**, 6976-6983.
4 X. Y. Ye, S. S. Rubakhin and J. V. Sweedler, *Analyst*, 2008, **133**, 423-433.
5 J. N. Wang, M. Q. Lu, F. Z. Yang, X. R. Zhang, W. R. G. Baeyens and A. M. G. Campana, *Anal. Chim. Acta*, 2001, **428**, 173-181.
6 W. Zhang, D. Zhao, R. Zhang, Z. Ye, G. Wang, J. Yuan and M. Yang, *Analyst*, 2011, **136**, 1867-1872.
7 J. H. Kim, D. A. Heller, H. Jin, P. W. Barone, C. Song, J. Zhang, L. J. Trudel, G. N. Wogan, S. R. Tannenbaum and M. S. Strano, *Nat. Chem.*, 2009, **1**, 473-481.
8 R. Miao, L. X. Mu, H. Y. Zhang, H. T. Xu, G. W. She, P. F. Wang and W. S. Shi, *J. Mater. Chem.*, 2012, **22**, 3348-3353.
9 Z. Shen, A. Webster, K. J. Welham, C. E. Dyer, J. Greenman and S. J. Haswell, *Analyst*, 2010, **135**, 302-305.
10 W. W. Li, X. M. Geng, Y. F. Guo, J. Z. Rong, Y. P. Gong, L. Q. Wu, X. M. Zhang, P. Li, J. B. Xu, G. S. Cheng, M. T. Sun and L. W. Liu, *ACS Nano*, 2011, **5**, 6955-6961.
11 K. J. Huang, M. Zhang, W. Z. Xie, H. S. Zhang, Y. Q. Feng and H. Wang, *Anal. Chim. Acta*, 2007, **591**, 116-122.
12 L. R. Cumba, J. P. Smith, D. A. C. Brownson, J. Iniesta, J. P. Metters, D. R. do Carmo and C. E. Banks, *Analyst*, 2015, **140**, 1543-1550.
13 B. R. Adhikari, M. Govindhan and A. C. Chen, *Electrochim. Acta*, 2015, **162**, 198-204.
14 B. R. Adhikari, M. Govindhan and A. C. Chen, *Sensors*, 2015, **15**, 22490-22508.
15 A. C. Chen and S. Chatterjee, *Chem. Soc. Rev.*, 2013, **42**, 5425-5438.
16 T. L. Xu, N. Scafa, L. P. Xu, L. Su, C. Z. Li, S. F. Zhou, Y. Liu and X. J. Zhang, *Electroanalysis*, 2014, **26**, 449-468.
17 B. J. Privett, J. H. Shin and M. H. Schoenfisch, *Chem. Soc. Rev.*, 2010, **39**, 1925-1935.
18 S. Kim, Y. Kim, Y. Ko and J. Cho, *J. Mater. Chem.*, 2011, **21**, 8008-8013.
19 X. Chen, H. Y. Long, W. L. Wu and Z. S. Yang, *Thin Solid Films*, 2009, **517**, 2787-2791.
20 Y. C. Liu, S. Q. Cui, J. Zhao and Z. S. Yang, *Bioelectrochemistry*, 2007, **70**, 416-420.
21 T. I. S. Oliveira, V. N. dos Santos, D. Lomonaco, A. N. Correia, S. E. Mazetto and P. de Lima-Neto, *J. Electrochem. Soc.*, 2013, **160**, B113-B118.
22 S. Griveau, C. Dumezy, J. Seguin, G. G. Chabot, D. Scherman and F. Bedioui, *Anal. Chem.*, 2007, **79**, 1030-1033.
23 W. W. Tu, J. P. Lei and H. X. Ju, *Electrochem. Commun.*, 2008, **10**, 766-769.
24 C. M. Yap, G. Q. Xu and S. G. Ang, *Anal. Chem.*, 2013, **85**, 107-113.
25 A. A. Abdelwahab, W. C. A. Koh, H.-B. Noh and Y.-B. Shim, *Biosens. Bioelectron.*, 2010, **26**, 1080-1086.
26 D. Zheng, C. Hu, Y. Peng, W. Yue and S. Hu, *Electrochem. Commun.*, 2008, **10**, 90-94.
27 C. X. Guo, S. R. Ng, S. Y. Khoo, X. T. Zheng, P. Chen and C. M. Li, *ACS Nano*, 2012, **6**, 6944-6951.
28 F. X. Hu, J. L. Xie, S. J. Bao, L. Yu and C. M. Li, *Biosens. Bioelectron.*, 2015, **70**, 310-317.
29 S. Thangavel and R. Ramaraj, *J. Phys. Chem. C*, 2008, **112**, 19825-19830.
30 D. A. C. Brownson and C. E. Banks, *Analyst*, 2011, **136**, 2084-2089.
31 J. J. Jiang and X. Z. Du, *Nanoscale*, 2014, **6**, 11303-11309.

32 A. Pandikumar, G. T. S. How, T. P. See, F. S. Omar, S. Jayabal, K. Z. Kamali, N. Yusoff, A. Jamil, R. Ramaraj, S. A. John, H. N. Lim and N. M. Huang, *RSC Adv.*, 2014, **4**, 63296-63323.

33 M. Regiart, S. V. Pereira, V. G. Spotorno, F. A. Bertolino and J. Raba, *Analyst*, 2014, **139**, 4702-4709.

34 S. S. Kumar and K. L. N. Phani, *J. Power Sources*, 2009, **187**, 19-24.

35 J. P. Wang, D. F. Thomas and A. C. Chen, *Chem. Commun.*, 2008, 5010-5012.

36 A. C. Chen and P. Holt-Hindle, *Chem. Rev.*, 2010, **110**, 3767-3804.

37 S. Jayabal, P. Viswanathan and R. Ramaraj, *RSC Adv.*, 2014, **4**, 33541-33548.

38 R. X. Xu, X. Y. Yu, C. Gao, J. H. Liu, R. G. Compton and X. J. Huang, *Analyst*, 2013, **138**, 1812-1818.

39 J. Yang and S. Gunasekaran, *Carbon*, 2013, **51**, 36-44.

40 J. Luo, M. M. Maye, V. Petkov, N. N. Kariuki, L. Y. Wang, P. Njoki, D. Mott, Y. Lln and C. J. Zhong, *Chem. Mater.*, 2005, **17**, 3086-3091.

41 C. V. Rao, C. R. Cabrera and Y. Ishikawa, *J. Phys. Chem. C*, 2011, **115**, 21963-21970.

42 D. J. Chen, Q. L. Zhang, J. X. Feng, K. J. Ju, A. J. Wang, J. Wei and J. J. Feng, *J. Power Sources*, 2015, **287**, 363-369.

43 A. C. Chen, D. J. La Russa and B. Miller, *Langmuir*, 2004, **20**, 9695-9702.

44 A. Sukeri, L. P. H. Saravia and M. Bertotti, *Phys. Chem. Chem. Phys.*, 2015, **17**, 28510-28514.

45 M. M. Maye, N. N. Kariuki, J. Luo, L. Han, P. Njoki, L. Y. Wang, Y. Lin, H. R. Naslund and C. J. Zhong, *Gold Bull.*, 2004, **37**, 217-223.

46 J. Suntivich, Z. C. Xu, C. E. Carlton, J. Kim, B. H. Han, S. W. Lee, N. Bonnet, N. Marzari, L. F. Allard, H. A. Gasteiger, K. Hamad-Schifferli and Y. Shao-Horn, *J. Am. Chem. Soc.*, 2013, **135**, 7985-7991.

47 J. D. Zhang and M. Oyama, *Anal. Chim. Acta*, 2005, **540**, 299-306.

48 A. C. A. de Vooys, G. L. Beltramo, B. van Riet, J. A. R. van Veen and M. T. M. Koper, *Electrochim. Acta*, 2004, **49**, 1307-1314.

49 M. Q. Xu, J. F. Wu and G. C. Zhao, *Sensors*, 2013, **13**, 7492-7504.

50 X. Zan, Z. Fang, J. Wu, F. Xiao, F. Huo and H. Duan, *Biosens. Bioelectron.*, 2013, **49**, 71-78.

51 S. L. Ting, C. X. Guo, K. C. Leong, D. H. Kim, C. M. Li and P. Chen, *Electrochim. Acta*, 2013, **111**, 441-446.

52 M. M. Shahid, P. Rameshkumar, A. Pandikumar, H. N. Lim, Y. H. Ng and N. M. Huang, *J. Mater. Chem. A*, 2015, **3**, 14458-14468.

53 C. M. Li, J. F. Zang, D. P. Zhan, W. Chen, C. Q. Sun, A. L. Teo, Y. T. Chua, V. S. Lee and S. M. Moochhala, *Electroanalysis*, 2006, **18**, 713-718.

54 N. Yusoff, A. Pandikumar, A. R. Marlinda, N. M. Huang and H. N. Lim, *Anal. Methods*, 2015, **7**, 3537-3544.

55 S. R. Ng, C. X. Guo and C. M. Li, *Electroanalysis*, 2011, **23**, 442-448.

56 F. H. Wu, G. C. Zhao and X. W. Wei, *Electrochem. Commun.*, 2002, **4**, 690-694.

57 Y. J. Li, C. Liu, M. H. Yang, Y. He and E. S. Yeung, *J. Electroanal. Chem.*, 2008, **622**, 103-108.

58 P. Kannan and S. A. John, *Electrochim. Acta*, 2010, **55**, 3497-3503.

59 A. Pandikumar and R. Ramaraj, *Indian J. Chem. A*, 2011, **50**, 1388-1393.

60 J. Hrbac, C. Gregor, M. Machova, J. Kralova, T. Bystron, M. Ciz and A. Lojek, *Bioelectrochemistry*, 2007, **71**, 46-53.

61 M. Zhu, M. Liu, G. Y. Shi, F. Xu, X. Y. Ye, J. S. Chen, L. T. Jin and J. Y. Jin, *Anal. Chim. Acta*, 2002, **455**, 199-206.

Graphical Abstract

A high-performance electrochemical sensor with AuPt nanoparticles and reduced graphene oxide nanocomposites is demonstrated for the effective detection of NO.

.